Regular article

Exploring the molecular mechanism of *Corydalis yanhusuo* against prostate cancer based on network pharmacology and molecular docking validation

Ying Zhu[a#], Junwei Lu[b#], Jumin Xie[a*]

[a] *Hubei Key Laboratory of Renal Disease Occurrence and Intervention, Medical school, Hubei Polytechnic University, Huangshi 435003, China;*
[b] *Department of Neurosurgery, Zhongnan Hospital of Wuhan University, Wuhan 430071, China*

Abstract

The molecular mechanism underlying *Corydalis Yanhusuo*'s therapeutic potential in prostate cancer (PCa) treatment was elucidated using network pharmacology and molecular docking. Nineteen active ingredients, 399 drug targets, 1790 disease targets and 143 intersection targets were identified. Ten core targets were screened from the protein-protein interaction network. Enrichment analysis revealed 133 GO terms and 114 KEGG pathways. *Corydalis Yanhusuo* may potentially treat prostate cancer through pathways such as the Rap1 signaling pathway, phospholipase D signaling pathway, Ras signaling pathway, VEGF signaling pathway and JAK-STAT signaling pathway. Significant differences in expression were observed for EGFR, PDGFRA, PIK3CA, PIK3CD, PIK3CG and PIK3R1. Molecular docking and dynamics simulation analysis showed low binding energy between active components and the six core genes of *Corydalis Yanhusuo*, indicating a favorable docking effect. This study shows that *Corydalis Yanhusuo* exhibits promise in prostate cancer treatment through a synergistic "multi-component-multi-target-multi-pathway" effect.

Keywords: *Corydalis Yanhusuo*; prostate cancer; network pharmacology; molecular mechanism; molecular docking

1 Introduction

Prostate cancer (PCa) is one of the most prevalent malignant tumors affecting the male reproductive system, especially in the elderly men, and it is characterized by significant heterogeneity [1]. The tumorigenesis of prostate cancer progresses through several stages, initial proliferation of luminal cells and ductal dysplasia, subsequent neoplastic changes in the prostate epithelium, and eventual development into localized prostate cancer. With the deterioration of basal cell layer and the invasion of cancer cells the disease develops into locally invasive prostate cancer. Ultimately, cancer cells may metastasize to lymph nodes, bones, liver and lungs, resulting in metastatic prostate cancer (mCRPC) [1].

Early-stage prostate cancer typically shows

# These authors contribute equally.
* Author to whom correspondence should be addressed. Address: Hubei key laboratory of renal disease occurrence and intervention, medical school, Hubei Polytechnic University. Guilin North Road No 16, Huangshi 435003, China. Tel.: +86-13871025626; E-mail: xiejumin@hbpu.edu.cn, xiejm922@163.com.

Received: 2024-06-30 Accepted: 2024-09-19

few symptoms, whereas advanced stages shows compressive symptoms, such as difficulty in urinating, frequent urination, urgency, increased nocturia, urinary incontinence, defecation difficulty, intestinal obstruction, insufficient ejaculation, and genital pain, and metastatic symptoms including hematuria, spermatorrhea, impotence, edema of the lower limbs, bone pain, pathological fractures, paraplegia, anemia and decreased blood count [2-5].

The International Agency for Research on Cancer (IARC), affiliated to the World Health Organization (WHO), analyzed 36 types of cancers across 185 countries in 2022. Their findings show that prostate cancer is the fourth most common cancer globally, following lung cancer, breast cancer and colorectal cancer. Among men, prostate cancer stands as the second most frequently diagnosed cancer, with the incidence second only to lung cancer [6].

Currently, screening and diagnosis of prostate cancer primarily involve methods such as prostate-specific antigen (PSA) testing, digital rectal examination, prostate Magnetic resonance imaging (MRI) and biopsy. Treatment options include active surveillance, radical prostatectomy, cryotherapy, radium-223 therapy, androgen deprivation therapy, radiotherapy and chemotherapy. However, these treatments may damage immunity and affect patients' daily life [7].

The combination of traditional Chinese medicine and Western medicine offers a "multi-component-multi-target-multi-pathway" approach to combat cancer. This combination therapy shows promising efficacy, affordability and minimal side effects, garnering significant attention from patients and researchers.

Yanhusuo, also known as Yuanhu, refers to the dried tuber of *Corydalis yanhusuo*, a plant belonging to the *Papaveraceae* family and *Corydalis* genus. It is widely used in traditional Chinese medicine. The earliest documented medicinal use of Yanhusuo in Chinese history dates back to the Northern and Southern Dynasties period. "*Lei Gong Pao Zhi Lun*" mentions "Die of heartache, find Yanhusuo quickly", and the name "Yanhusuo" first appeared in the Tang Dynasty. According to "*Bencao Shi Yi*", Yanhusuo originated from Xi Guo and Andong, similar to the root of *Pinellia ternata* and its color is yellow [8,9]. Historical records of various dynasties indicate that Yanhusuo promotes blood circulation, regulates qi and alleviates pain. It is commonly prescribed for conditions such as chest and rib pain, menstrual disorders and postpartum blood stasis.

Modern research has identified several pharmacological effects of Yanhusuo, including anti-inflammatory [10], analgesic [11,12], sedative-hypnotic [13], myocardial protection [14], drug detoxification [15], anti-intestinal and gastric ulcer [16] and anti-tumor properties [17,18]. Yanhusuo is extensively utilized in clinical practice for treating gynecological diseases, skin conditions, neurological disorders, arthralgia, digestive disorders and other ailments, demonstrating notable therapeutic efficacy [19]. Currently, Yanhusuo is also being studied for its potential to enhance brain function and lower cholesterol and blood lipid levels, among other functions. However, research on Yanhusuo's effects against prostate cancer remains limited [16].

In this study, an interactive "component-target-pathway" network between *Corydalis yanhusuo* and prostate cancer was established by using network pharmacology and molecular docking technology. The potential mechanisms by which *Corydalis yanhusuo* treats prostate cancer was also investigated to provide a theoretical foundation for developing new clinical treatments. The flowchart of this research is shown in Fig. 1.

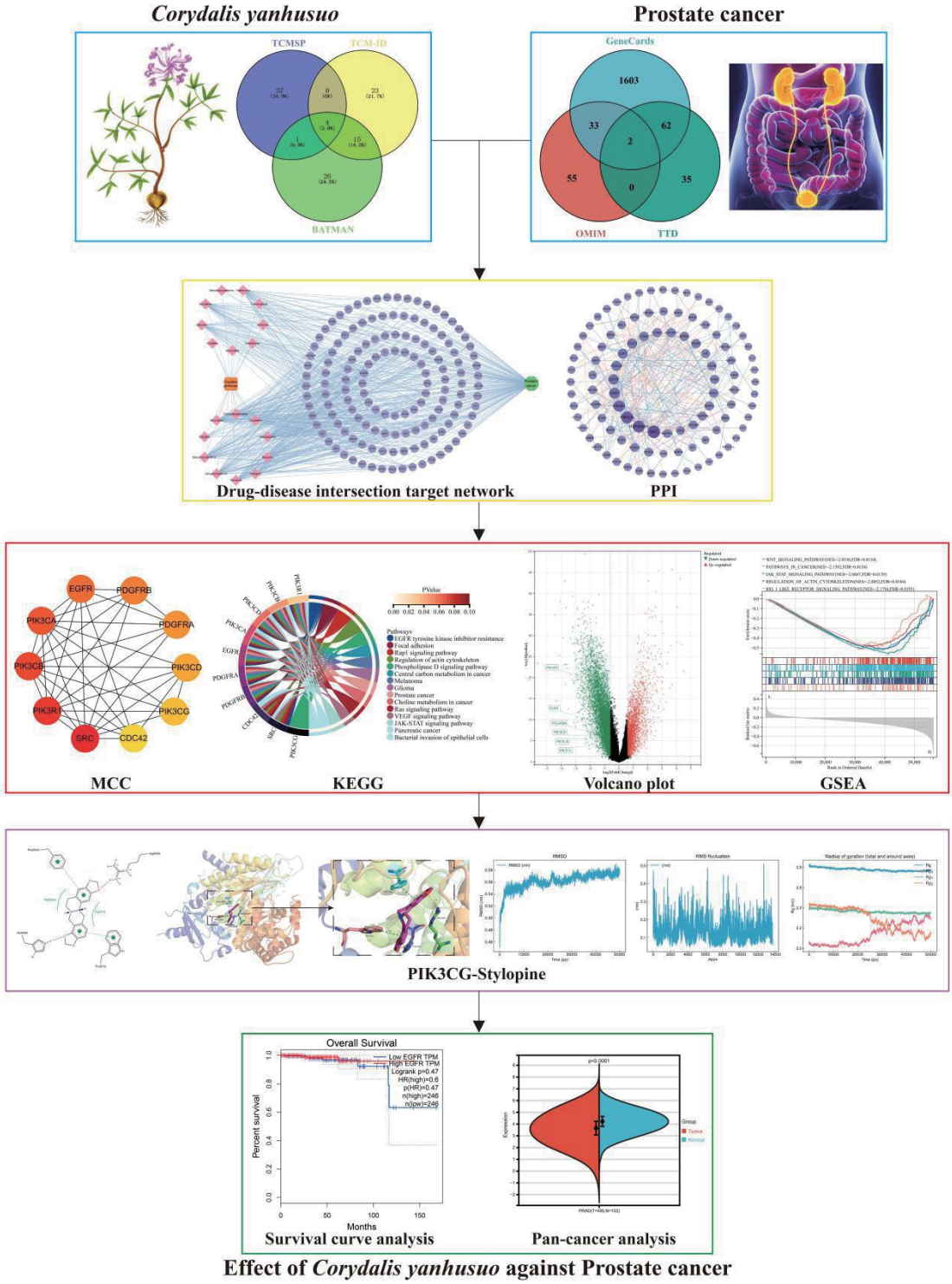

Fig. 1 Flowchart of the study of *Corydalis yanhusuo* against prostate cancer

2 Materials and methods

2.1 Active ingredients screening of Corydalis yanhusuo and target prediction

The active ingredients of *Corydalis yanhusuo* were identified by searching Traditional Chinese Medicine Systems Pharmacology (TCMSP) [20] (https://old.tcmsp-e.com/), Traditional Chinese Medicine Information Database (TCM-ID) [21] (http://bidd.group/TCMID/), and Bioinformatics Analysis Tool for Molecular mechANism of Traditional Chinese Medicine (BATMAN-TCM) [22] (http://bionet.ncpsb.org.cn/batman-tcm/) and using the keyword "*Corydalis yanhusuo*". Initial screening in the TCMSP database was based on criteria of oral bioavailability (OB) ≥ 30% and drug-like properties (DL) ≥ 0.18 [23]. The intersection of these results was determined using Venny2.1.0 (https://bioinfogp.cnb.csic.es/tools/venny/).

Isomeric SMILES identifiers for these components were retrieved from PubChem [24] (https://pubchem.ncbi.nlm.nih.gov), and drug candidates from TCMSP, TCM-ID, and BATMAN-TCM were re-evaluated using the SwissADME [25] (http://www.swissadme.ch/) platform. Screening criteria included high gastrointestinal absorption (GI absorption, GI) and adherence to drug-likeness rules, namely molecular weight ≤ 500, iLOGP ≤ 5, H-bond donors ≤ 5, and hydrogen bond acceptors ≤ 10. As a result, effective drug active ingredients were identified from *Corydalis yanhusuo*.

The 2D structures of these selected active ingredients were obtained from the PubChem database and downloaded in SDF format. Target prediction for these active ingredients was conducted using the Swiss Target Prediction [26] (http://www.swisstargetprediction.ch) database, with "Homo sapiens" as the species and screening criteria set to "Probability > 0.1".

2.2 Prostate cancer-related targets collection

Utilizing three disease databases, GeneCards [27] (https://www.genecards.org/), Online Mendelian Inheritance in Man (OMIM) [28] (https://www.omim.org/), and Therapeutic Target Database (TTD) [29] (https://db.idrblab.net/ttd/), with "*Homo sapiens*" specified as the organism and "Prostate cancer" as the keyword, gene targets associated with prostate cancer were retrieved.

In the GeneCards database, targets were screened based on their Relevance score value. Targets obtained from OMIM and TTD databases were integrated using the Hiplot (https://hiplot.cn/basic) website to compile a comprehensive list of prostate cancer-related targets.

2.3 Drug-disease intersection target network construction

The intersection of predicted targets involving effective components of *Corydalis yanhusuo* and prostate cancer-related targets was determined using Hiplot. This analysis identified the specific targets through which *Corydalis yanhusuo* may act against prostate cancer. Subsequently, Type and Network tables were generated and imported into Cytoscape 3.9.0 software to visualize a network diagram depicting the relationships among "*Corydalis yanhusuo*-components-prostate cancer-targets".

2.4 Protein-protein interaction (PPI) network construction

The intersection targets of *Corydalis yanhusuo* and prostate cancer were uploaded to the Search Tool for the Retrieval of Interaction Gene/Proteins (STRING) [30] (https://cn.string-db.org/) database with a confidence score threshold of 0.95. Non-significant targets were then filtered out to generate a protein interaction map, saved in TSV format

and imported into Cytoscape 3.9.0 software for visualization. This facilitated the construction of a protein-protein interaction (PPI) network.

To identify core targets, the Maximal Clique Centrality (MCC) algorithm of the Cytohubba plugin within Cytoscape software was utilized [31]. The core target interactions were screened and subsequently uploaded back into the STRING database to produce a refined core target protein interaction map.

2.5 GO function and KEGG pathway enrichment analysis

The core targets were uploaded to the DAVID [32] (https://david.ncifcrf.gov/) database for Gene Ontology (GO) functional analysis and Kyoto Encyclopedia of Genes and Genomes (KEGG) pathway enrichment analysis, restricting the species to "*Homo sapiens*". Targets for GO biological processes (GO-BP), cellular components (GO-CC), molecular functions (GO-MF) and KEGG pathways were obtained. The GO-BP/CC/MF data were arranged in descending order of *P*-Value, and the top 10 pathways were used to generate a Sankey diagram using the Bioinformatics platform (https://www.bioinformatics.com.cn/). The top 15 pathways identified from KEGG enrichment were then imported into the SangerBox (http://sangerbox.com/) website to create a string diagram.

2.6 Genetic difference analysis

The clinical data for Prostate adenocarcinoma (PRAD) from The Cancer Genome Atlas (TCGA) and the "RNA-Seq-HTSeq-FPKM" expression profiles were retrieved using the SangerBox website. The difference of gene expression between prostate cancer and adjacent tissues was examined to identify differential genes, which were then intersected with core targets to determine the differential core targets.

A volcano plot depicting these differential core targets was generated on the SangerBox website. Subsequently, Gene Set Enrichment Analysis (GSEA) was conducted on these targets. Pathways showing significant enrichment were selected based on the following criteria: |NES| > 1, NOM p-val < 0.05, and FDR q-val < 0.25. The top 5 pathways, in which these genes are notably enriched, were shown.

2.7 Molecular docking, dynamics simulation and visualization

To investigate potential interaction between core targets and active ingredients, differentially expressed core targets were queried in the protein database Universal Protein (Uniprot) [33] (https://www.uniprot.org/), focusing on "Reviewed" entries for human proteins. Relevant target entries were then searched in the RCSB Protein Data Bank (PDB) [34] database (https://www.rcsb.org/) to identify crystal structures of target proteins meeting specific criteria: human origin, near full-length sequence, few unique ligands and a small number of modifications.

Meanwhile, the 2D structure of the effective components from *Corydalis yanhusuo* was retrieved from the PubChem database as small molecules. Initially, the structures of these small molecules were optimized using Chem 3D software and saved in mol2 format. Simultaneously, the macromolecule structures were processed using PyMOL to exclude water molecules and residues, and were converted into PDB format. AutoDockTools 1.5.7 software facilitated the preparation of both protein and small molecule structures in "pdbqt" format.

Subsequently, AutoDock Vina was employed to simulate the docking of protein-small molecule pairs and record the binding energy. Complexes with low binding energy and favorable conformation were selected for further analysis in PyMOL to verify bonding interaction. Binding energy data obtained from molecular docking were then uploaded to the

Cnsknowall (https://cnsknowall.com/#/HomePage) website and visualized in the form of heatmap.

In this study, OpenMM7 was used for molecular dynamics simulations [35]. Sobtop was employed to model the behavior of small molecules such as Coptistine, Dehydrocorydalmine, Bicuculline and Stylopine [36]. The FF14SB protein force field was utilized for the simulations [37]. GROMACS (version 2020.6) generated the necessary .gro and .top files for the complexes, and OpenMM7 was used for the simulations. Parameters included Hydrogen Mass (amu) = 1.0, Step Size (ps) = 0.002, Temperature (K) = 310, and Equilibration Length (steps) = 10,000. OpenMM7 performed energy minimization followed by simulations up to 50 nanoseconds. Post-simulation, root mean square fluctuation (RMSF), root mean square deviation (RMSD) and radius of gyration (Rg) were calculated. Visual results were generated using DuIvyTools (https://duivytools.readthedocs.io/en/latest/DIT.html).

2.8 Overall survival and pan-cancer analysis

We utilized the Gene Expression Profiling Interactive Analysis (GEPIA) (http://gepia.cancer-pku.cn/) website to perform survival curve analysis on the difference of core target gene expression between prostate cancer tissues and normal tissues. We assessed the hazard ratio (HR). If HR > 1, the gene is identified as a risk factor, indicating that elevated expression correlates with decreased patient survival rates. On the contrary, if HR < 1, the gene is considered a protective factor, suggesting that higher expression enhances patient survival rates.

Subsequently, we employed the SangerBox website to analyze gene differences among prostate cancer-related cell lines based on *P*-value.

3 Results

3.1 Main active ingredients of Corydalis yanhusuo and correlated targets

A total of 49 drug components were screened from the TCMSP database, 42 from the TCM-ID database, and 46 from the BATMAN-TCM database. The results from these three databases were intersected using Venny 2.1, resulting in the identification of 20 effective components of *Corydalis yanhusuo* (Fig. 2A). One component that could not be found in PubChem was subsequently removed, leaving a total of 19 effective components (Table 1). The molecular structures of these components were shown in Fig. 3. Target prediction analysis was conducted on these components, yielding 399 predicted targets.

3.2 Prostate cancer targets

We retrieved 13,594 prostate cancer targets from the GeneCards database, and selected 1,700 targets based on Relevance scores surpassing the median value. Integrating targets from the TTD and OMIM databases using Hiplot resulted in a final set of 1,790 prostate cancer targets (Fig. 2B).

3.3 "Corydalis yanhusuo-components-prostate cancer" network construction

The intersection of 1,790 prostate cancer targets with 399 predicted targets of *Corydalis yanhusuo* yielded 143 disease-drug intersection targets (Fig. 4A). The Type and Network information tables of these intersection targets were imported into Cytoscape 3.9.0 software to construct a network depicting "*Corydalis yanhusuo*-components-prostate cancer" (Fig. 4B).

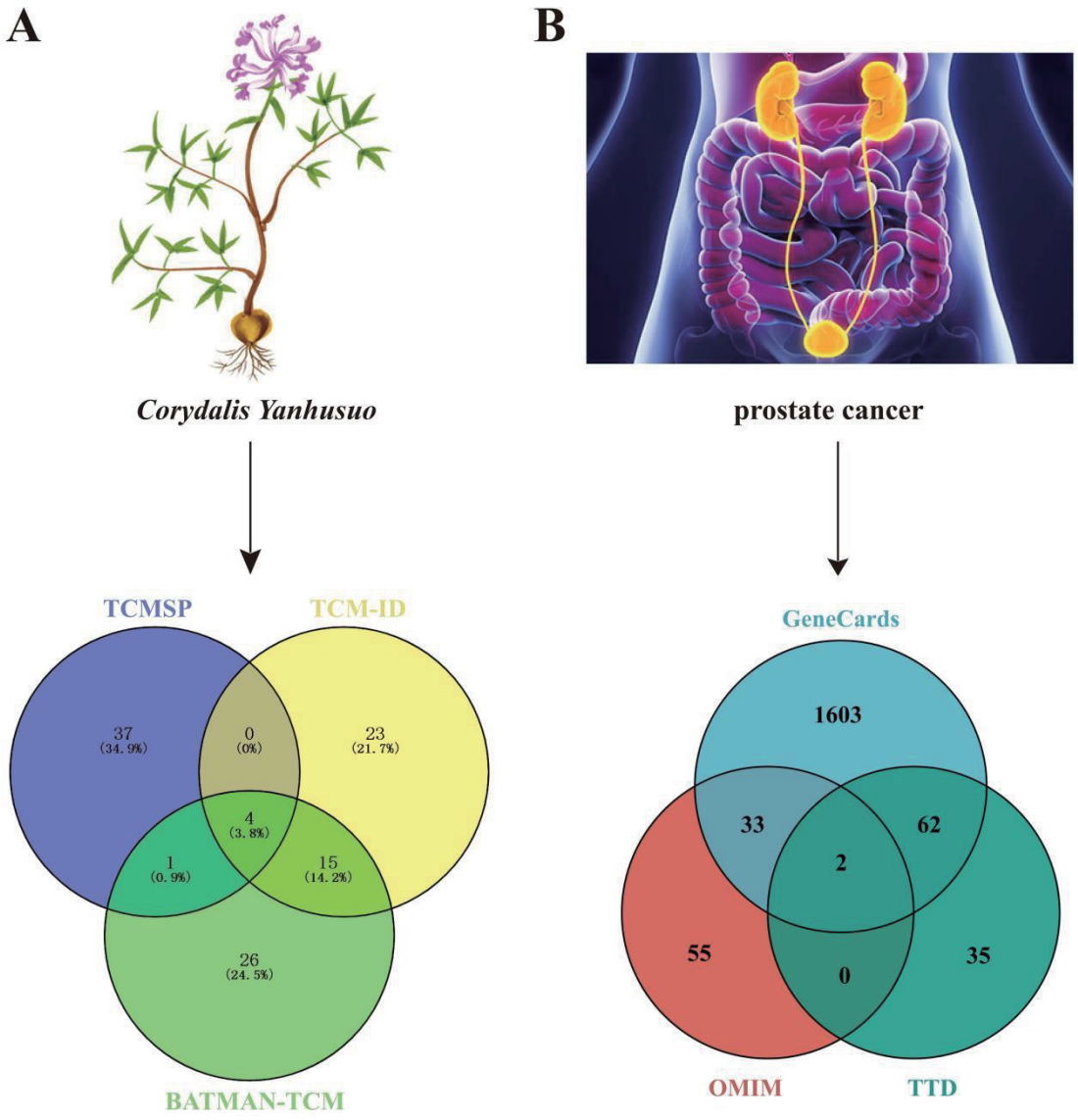

Fig. 2 Analysis of *Corydalis yanhusuo*-target-prostate cancer. (A) Target of *Corydalis yanhusuo*; (B) Target of prostate cancer

3.4 PPI network construction

143 disease-drug intersection targets were uploaded to the STRING website with a confidence level of 0.95. After removing 11 non-specific targets, a protein interaction map of the remaining targets was generated. The map was saved in TSV format and imported into Cytoscape 3.9.0 software. Using the "Analyze network" function, topological properties were calculated, revealing 101 nodes and 284 edges (Fig. 5A). Nodes were sorted by degree values, with larger circle areas indicating higher degree values and reflecting stronger gene target interactions.

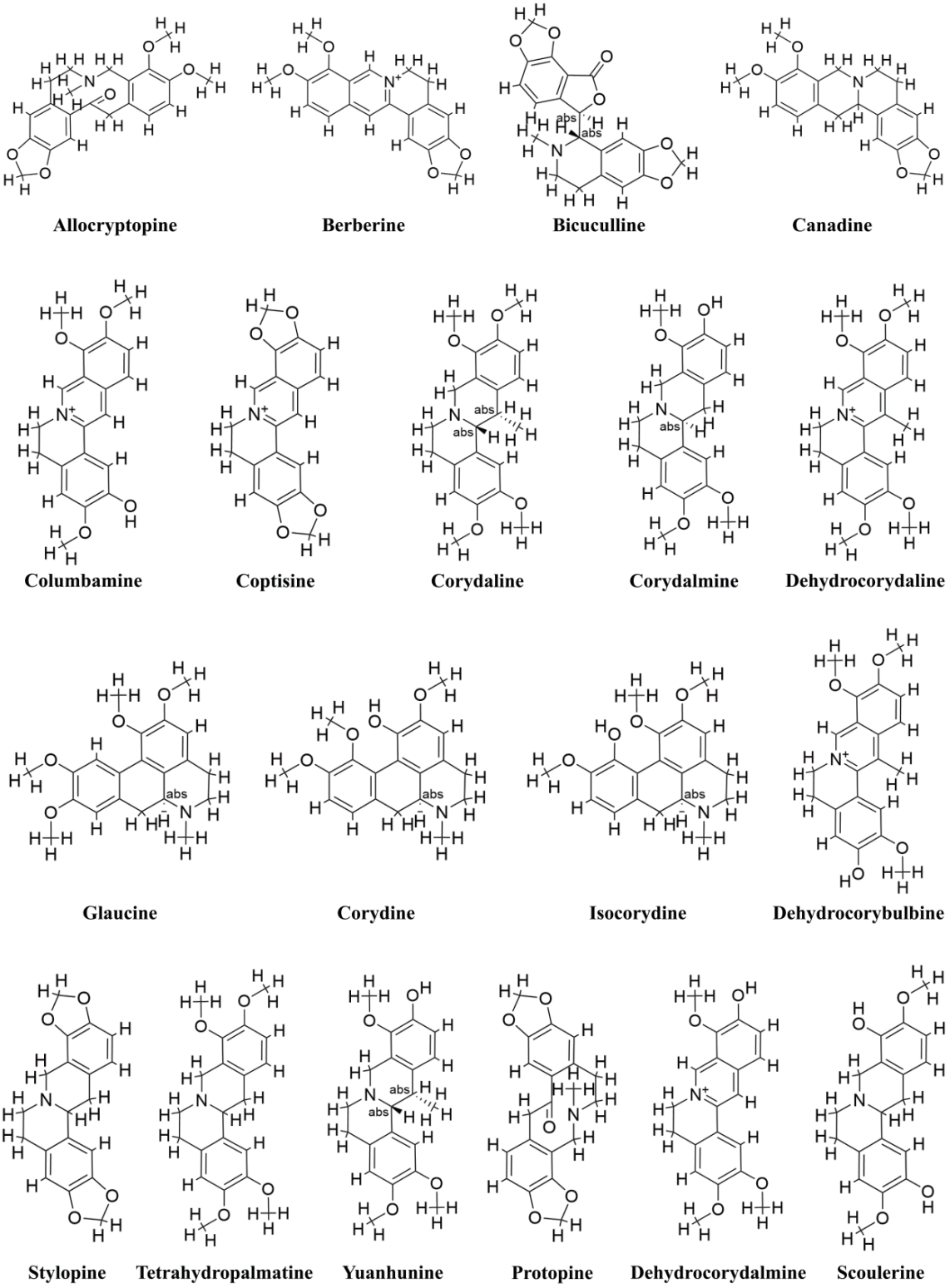

Fig. 3 Molecular structure of the 19 active ingredients in *Corydalis yanhusuo*

Table 1 Detailed information of the active components in *Corydalis yanhusuo*

No.	CAS ID	Molecule Name	Formula	MW (g/mol)
1	476-69-7	Corydine	$C_{20}H_{23}NO_4$	341.4
2	59870-72-3	Dehydrocorybulbine	$C_{21}H_{22}NO_4^+$	352.4
3	6877-27-6	Dehydrocorydalmine	$C_{20}H_{20}NO_4^+$	338.4
4	30413-84-4	Corydalmine	$C_{20}H_{23}NO_4$	341.4
5	104387-15-7	Yuanhunine	$C_{21}H_{25}NO_4$	355.4
6	3621-36-1	Columbamine	$C_{20}H_{20}NO_4^+$	338.4
7	485-49-4	Bicuculline	$C_{20}H_{17}NO_6$	367.4
8	3486-66-6	Coptisine	$C_{19}H_{14}NO_4^+$	320.3
9	518-69-4	Corydaline	$C_{22}H_{27}NO_4$	369.5
10	30045-16-0	Dehydrocorydaline	$C_{22}H_{24}NO_4^+$	366.4
11	130-86-9	Protopine	$C_{20}H_{19}NO_5$	353.4
12	2086-83-1	Berberine	$C_{20}H_{18}NO_4^+$	336.4
13	605-34-5	Scoulerine	$C_{19}H_{21}NO_4$	327.4
14	475-67-2	Isocorydine	$C_{20}H_{23}NO_4$	341.4
15	485-91-6	Allocryptopine	$C_{21}H_{23}NO_5$	369.4
16	4312-32-7	Stylopine	$C_{19}H_{17}NO_4$	323.3
17	522-97-4	Canadine	$C_{20}H_{21}NO_4$	339.4
18	2934-97-6	Tetrahydropalmatine	$C_{21}H_{25}NO_4$	355.4
19	475-81-0	Glaucine	$C_{21}H_{25}NO_4$	355.4

MCC algorithm of the Cytohubba plugin in Cytoscape was employed to identify 10 core targets, Phosphatidylinositol-4,5-Bisphosphate 3-Kinase Catalytic Subunit Delta (PIK3CD), Platelet Derived Growth Factor Receptor Alpha (PDGFRA), Proto-oncogene tyrosine-protein kinase Src (SRC), Phosphatidylinositol-4,5-Bisphosphate 3-Kinase Catalytic Subunit Alpha (PIK3CA), EGFR (Epidermal growth factor receptor), Platelet Derived Growth Factor Receptor Beta (PDGFRB), Phosphoinositide-3-Kinase Regulatory Subunit 1 (PIK3R1), Phosphatidylinositol-4,5-Bisphosphate 3-Kinase Catalytic Subunit Beta (PIK3CB), Cell Division Cycle 42 (CDC42) and Phosphatidylinositol-4,5-Bisphosphate 3-Kinase Catalytic Subunit Gamma (PIK3CG). A core target network was visualized, highlighting more significant genes with darker colors. These core targets were then analyzed on the STRING website to generate a protein interaction map (Fig. 5B).

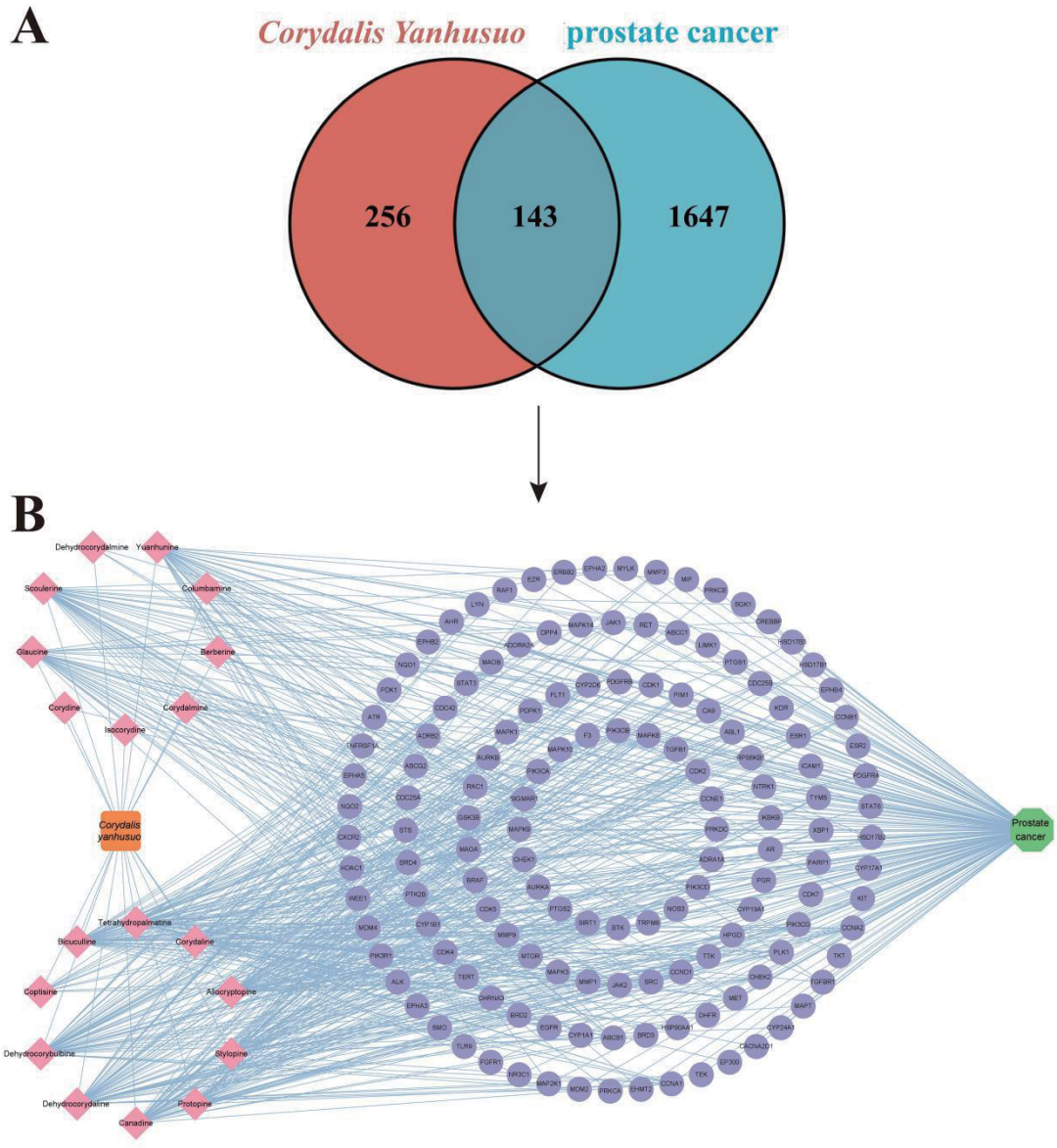

Fig. 4 Targets of *Corydalis yanhusuo* against prostate cancer. (A) Intersection targets of *Corydalis yanhusuo* and prostate cancer; (B) Network of *Corydalis yanhusuo*-components-prostate cancer

3.5 GO function and KEGG pathway enrichment analysis

The 10 core targets were inputted into the DAVID database, utilizing GO-BP, GO-CC and GO-MF to identify 91, 17 and 25 pathways respectively. The top 10 pathways with the highest significance were chosen for the sankey diagram (Fig. 6A-C). Analysis revealed that, biologically, these targets predominantly functioned in positive regulation of protein kinase B signaling, phosphatidylinositol-mediated signaling, phosphatidylinositol 3-kinase signaling and phosphatidylinositol phosphorylation. In terms of cellular localization, they are primarily located in the cytoplasm, cell membrane and plasma membrane. Regarding molecular function, ATP

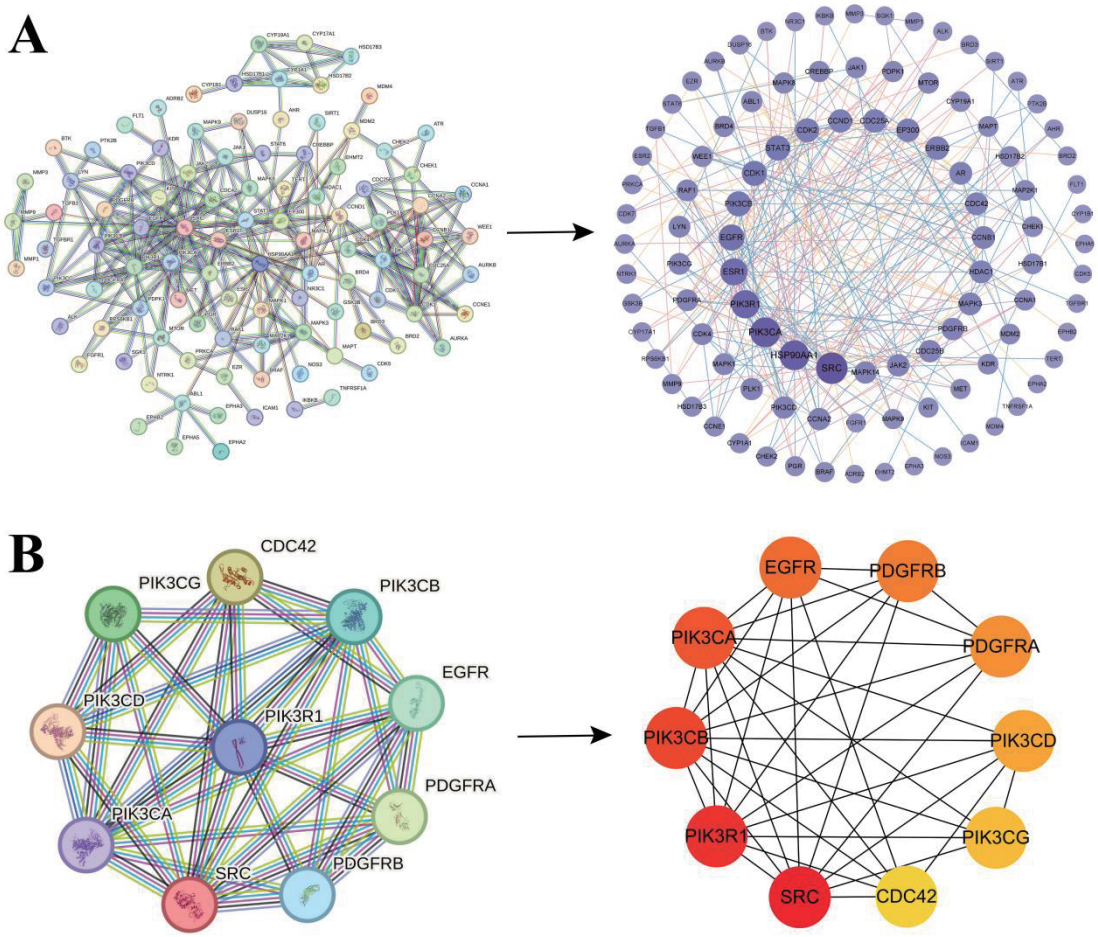

Fig. 5 Targets and core targets of *Corydalis yanhusuo* against prostate cancer. (A) PPI network and visualization of *Corydalis yanhusuo* against prostate cancer; (B) PPI network and visualization of the core targets

binding emerged as a significant function.

Furthermore, KEGG enrichment identified 114 pathways, with the top 15 pathways of highest significance selected for string diagram analysis (Fig. 6D). The analysis indicated that the core targets involved in treating prostate cancer with *Corydalis yanhusuo* were primarily related to pathways such as the Rap1 signaling pathway, phospholipase D signaling pathway, central carbon metabolism in cancer, choline metabolism in cancer, Ras signaling pathway, VEGF signaling pathway and JAK-STAT signaling pathway.

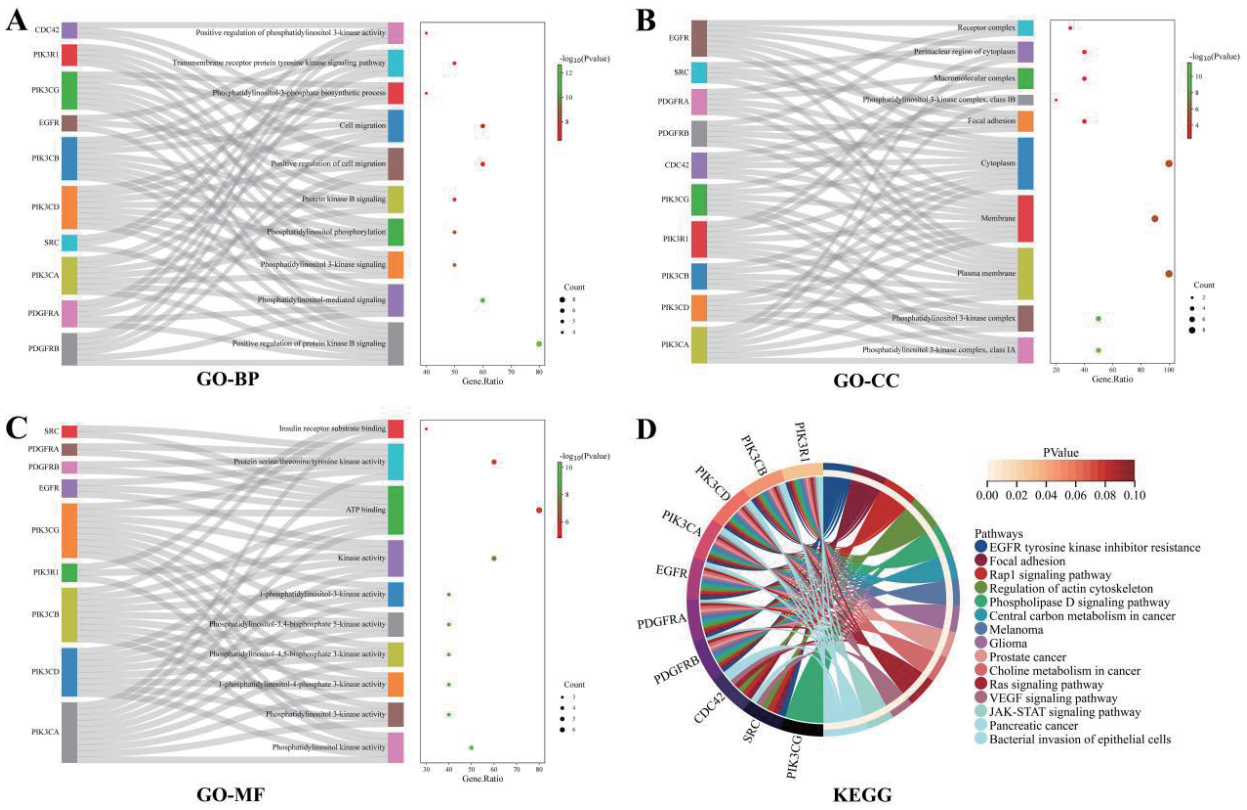

Fig. 6 GO function and KEGG enrichment analysis of targets in *Corydalis yanhusuo* against prostate cancer. (A) Biological process (BP) enrichment analysis of targets of *Corydalis yanhusuo* against prostate cancer; (B) Molecular function (MF) enrichment analysis of targets of *Corydalis yanhusuo* against prostate cancer; (C) Cellular component (CC) enrichment analysis of targets of *Corydalis yanhusuo* against prostate cancer; (D) String diagram of the top 15 pathways of KEGG enrichment analysis of targets of *Corydalis yanhusuo* against prostate cancer

3.6 Genetic difference analysis

On Sangerbox website, 9,275 differentially expressed genes were analyzed, and their intersection with the core targets revealed six differentially expressed core targets: EGFR, PDGFRA, PIK3CA, PIK3CD, PIK3CG and PIK3R1. These six core targets were depicted in a volcano plot on the Sangerbox website (Fig. 7), indicating significant down-regulation. GSEA analysis (Fig. 8) demonstrated that these genes were notably enriched in cancer pathways, actin filament regulation in the cytoskeleton, JAK-STAT signaling pathway, RIG-I-like receptor signaling pathway, MAPK signaling pathway and Wnt signaling pathway.

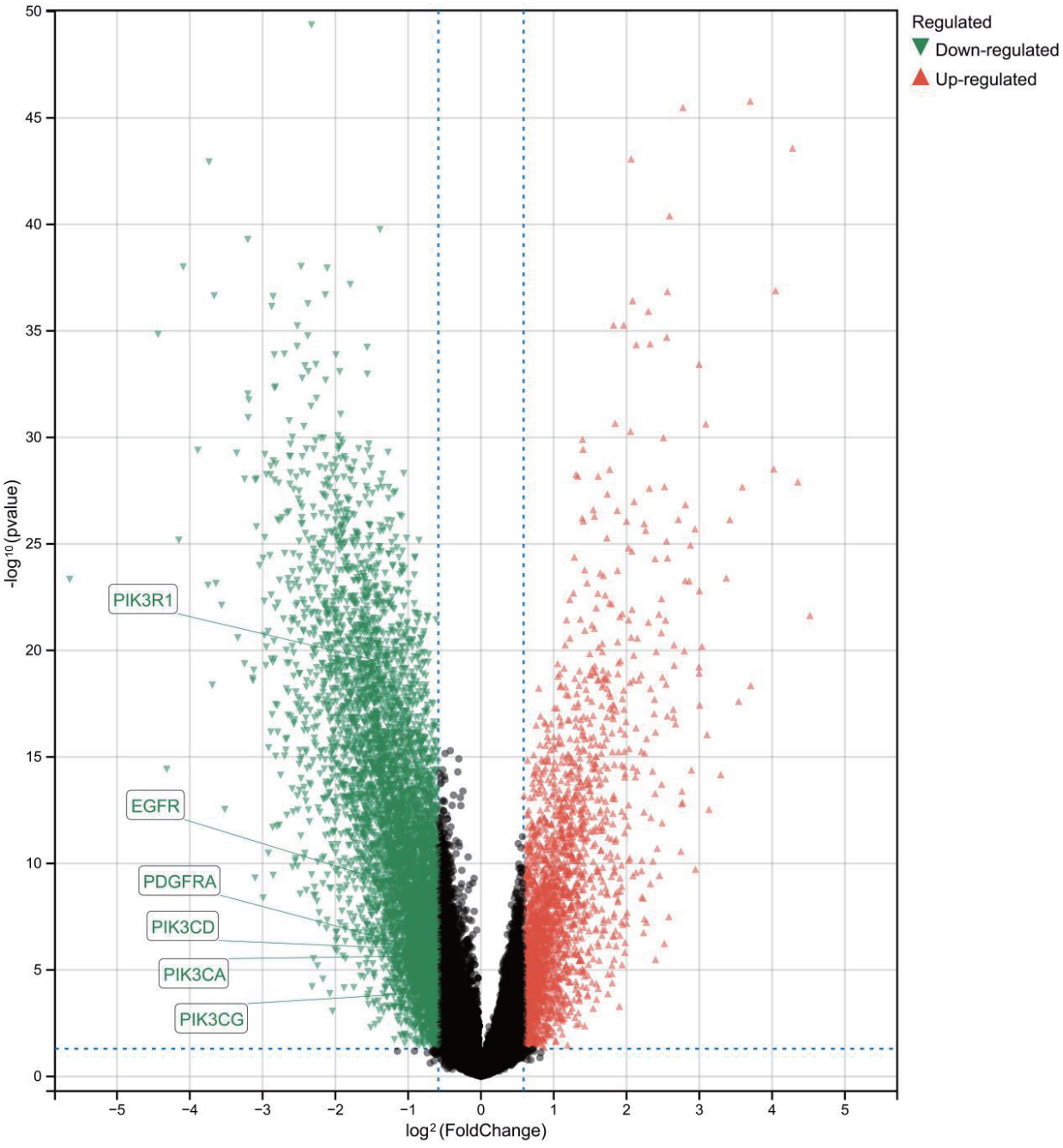

Fig. 7 Volcano plot of differentially expressed genes in prostate cancer from the TCGA database

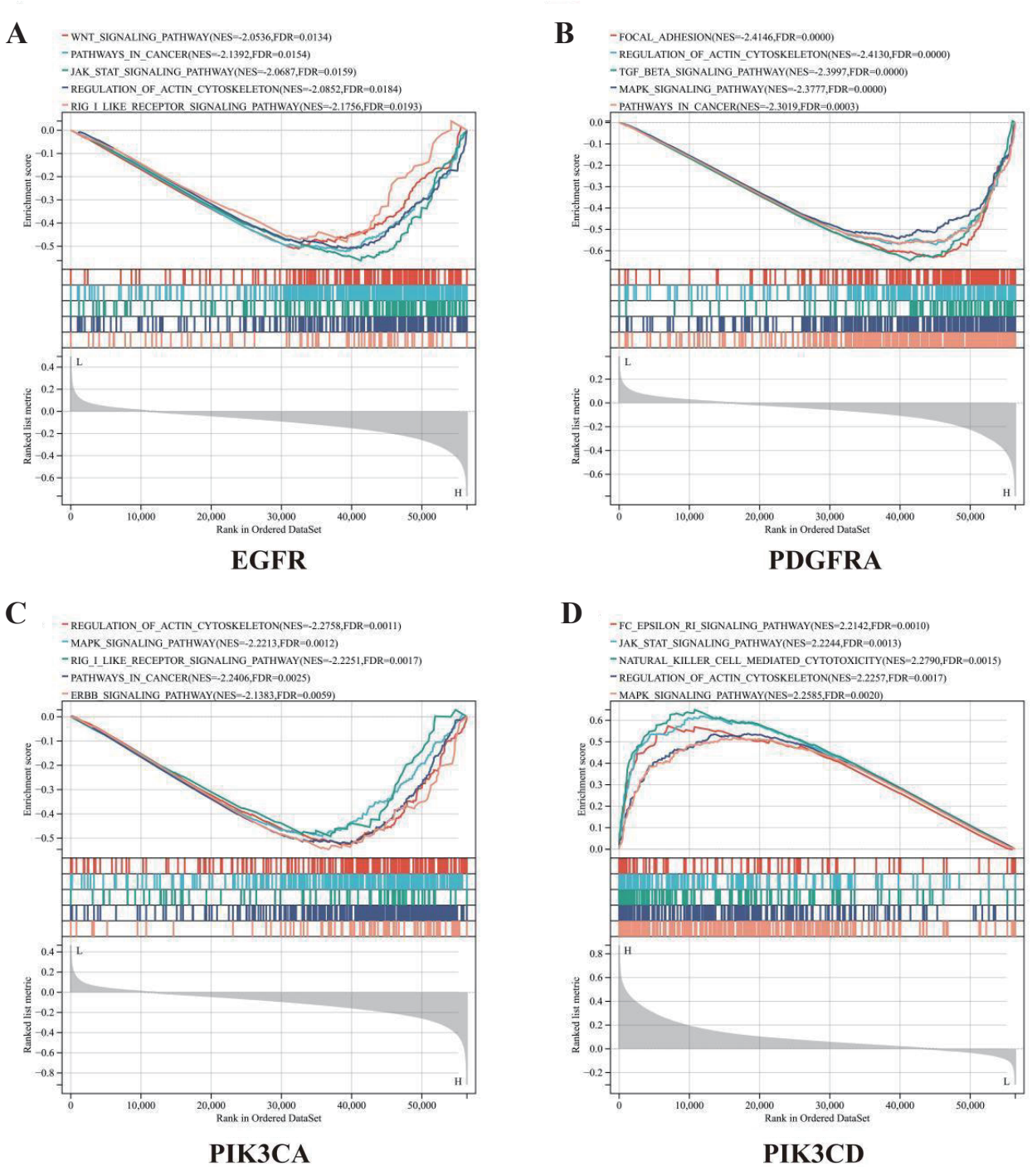

Fig. 8 GSEA enrichment analysis of six differential expressed genes. (A-F) EGFR, PDGFRA, PIK3CA, PIK3CD, PIK3CG, and PIK3R1

(to be continued)

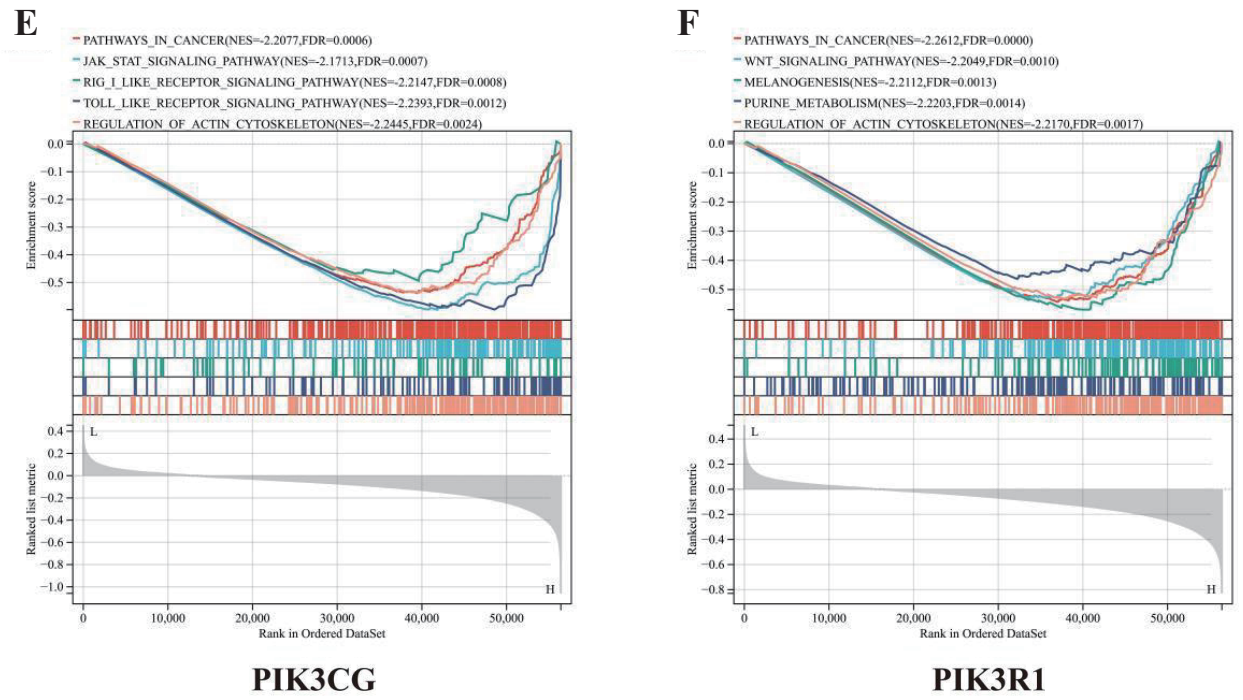

Continued Fig. 8

3.7 Molecular docking, dynamics simulation and visualization

In the initial stages, six core targets—EGFR, PDGFRA, PIK3CA, PIK3CD, PIK3CG and PIK3R1—were queried in the RCSB PDB database to identify macromolecules. These six macromolecules, along with 19 small molecules, underwent molecular docking using AutoDockTools 1.5.7 software and Autodock Vina. The binding energy data were visualized as a heatmap on Cnsknowall website (Fig. 9).

Subsequently, the combinations with the lowest binding energy (Table 2) were chosen for molecular visualization, namely, PDGFRA-Coptisine, PDGFRA-Dehydrocorydalmine, PIK3CA-Bicuculline, PIK3CA-Coptisine and PIK3CG-Stylopine (Fig. 10A-E). The molecular dynamics simulation results revealed stable binding between Bicuculline and PI3KCA, though the binding exhibited some fluctuations. The RMSD curve demonstrated the binding stability of the PI3KCA-Bicuculline complex over 50 ns (Fig. 10L). The RMSF curve showed the minimal fluctuation in the PI3KCA protein, indicating the stability of its domain and conserved functional regions (Fig. 10M). The Rg curve remained stable throughout the simulation, reflecting the structural integrity of the PI3KCA-Bicuculline complex (Fig. 10N). For the PI3KCA-Stylopine complex, stable binding was also observed, with the RMSD curve indicating a consistent interaction between Stylopine and PI3KCA (Fig. 10R). The RMSF curve showed little fluctuation in PI3KCA, suggesting domain stability and conserved functional regions (Fig. 10S). The Rg curve remained stable, indicating the structural integrity of the complex (Fig. 10T). However, the simulations for the remaining three complexes, PDGFRA-Coptistine, PDGFRA-Dehydrocorydalmine and PI3KCA-Coptistine, did not achieve stable binding within 50 ns (Fig. 10F-H, I-K, O-Q).

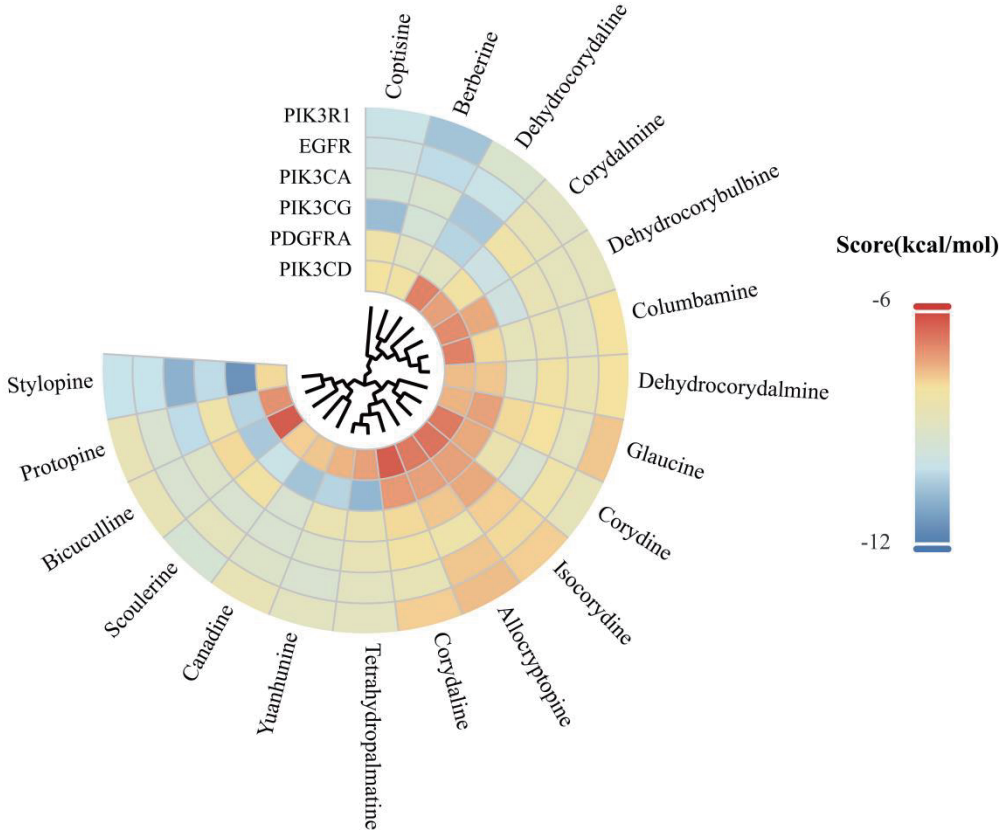

Fig. 9 Heat map of molecular docking results

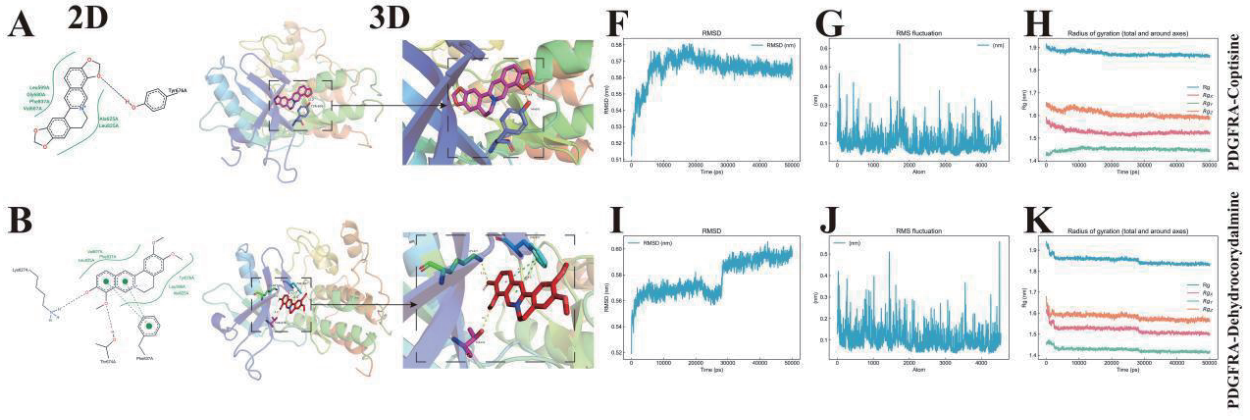

Fig. 10 Visualization of the molecular docking and dynamics simulation complexes. (A-E) 2D and 3D structure of PDGFRA-Coptisine, PDGFRA-Dehydrocorydalmine, PIK3CA-Bicuculline, PIK3CA-Coptisine, and PIK3CG-Stylopine. (F-T) RMSD, RMSF, and Rg curves of PDGFRA-Coptisine, PDGFRA-Dehydrocorydalmine, PIK3CA-Bicuculline, PIK3CA-Coptisine, and PIK3CG-Stylopine

(to be continued)

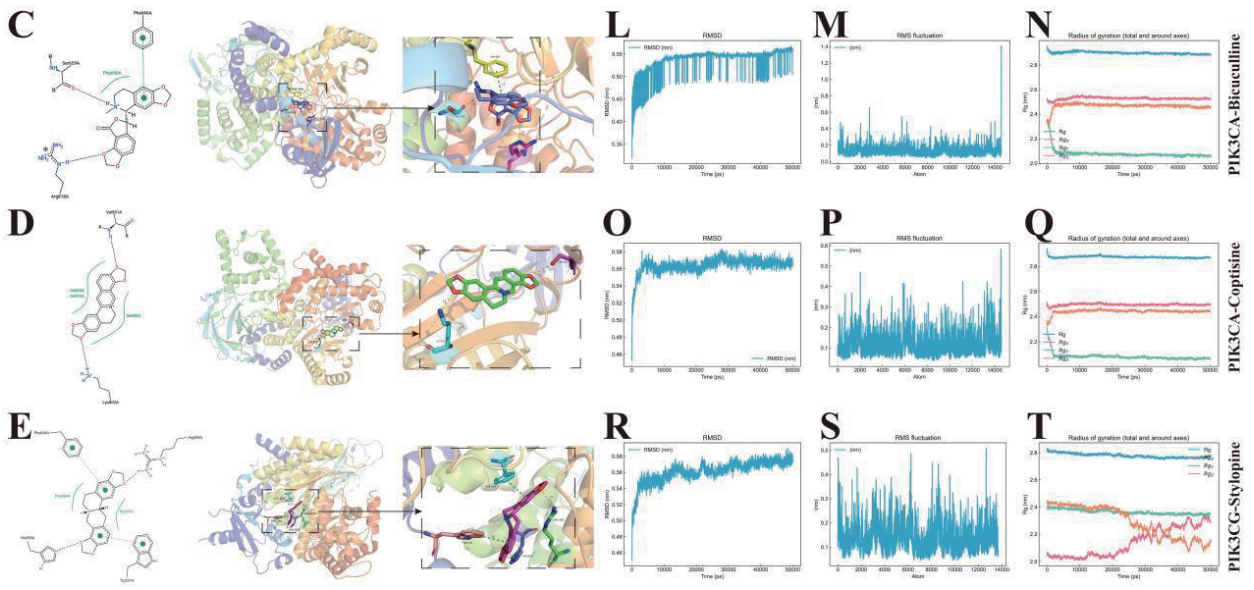

Continued Fig. 10

Table 2 Molecular docking Binding energy

Score (kcal/mol)						
PDB	4I24	5GRN	8EXL	7EAL	6AUD	5GJI
Ingredients	EGFR	PDGFRA	PIK3CA	PIK3CD	PIK3CG	PIK3R1
Allocryptopine	-8.2	-7.4	-9.3	-6.8	-8.4	-8.7
Berberine	-9.3	-10.2	-10.1	-7.1	-8.2	-8.6
Bicuculline	-9.9	-8.9	-10.4	-6.9	-10.2	-9.2
Canadine	-8.8	-7.4	-8.6	-7.0	-9.7	-8.8
Columbamine	-9.3	-10.2	-9.1	-7.5	-8.5	-8.9
Coptisine	-10	-11.4	-10.8	-7.9	-10.1	-10
Corydaline	-8.8	-7.3	-8	-7.5	-7.9	-7.7
Corydalmine	-8.8	-9.9	-9.3	-7.8	-8.1	-9.4
Corydine	-7.7	-7.3	-8.3	-6.8	-7.7	-7.6
Dehydrocorybulbine	-9.1	-10.5	-9.3	-7.7	-9.3	-8.6
Dehydrocorydaline	-9.3	-10.4	-9.1	-6.4	-7.9	-8.6
Dehydrocorydalmine	-8.9	-10.7	-8.6	-7.3	-8.4	-8.9

(to be continued)

Continued Table 2

	Score (kcal/mol)					
Glaucine	-8.6	-7.2	-8.1	-6.4	-7.9	-7.8
Isocorydine	-7.9	-7.3	-7.8	-6.7	-7.4	-7.8
Protopine	-10.1	-8.9	-9.2	-8.1	-9.5	-10.5
Scoulerine	-8.6	-8.1	-8.2	-7.3	-9.8	-9
Stylopine	-9.8	-8.2	-9.5	-8.0	-10.6	-9.9
Tetrahydropalmatine	-8.5	-7.7	-8.1	-7.6	-9.1	-8
Yuanhunine	-8.9	-7.9	-8.5	-6.9	-8.7	-8

3.8 Overall survival and pan-cancer analysis

Six core targets were analyzed on the GEPIA website to generate survival curves (Fig. 11). The risk ratios of PIK3CA and PIK3CD were greater than 1, whereas the risk rations of EGFR, PDGFRA, PIK3CG and PIK3R1 were less than 1. Predictive modeling suggested that upregulating EGFR, PDGFRA, PIK3CG and PIK3R1 and downregulating PIK3CA and PIK3CD might prolong the survival time of prostate cancer patients.

In the SangerBox biomedical data analysis platform, differential expression analysis of EGFR, PDGFRA, PIK3CA, PIK3CD, PIK3CG and PIK3R1 genes was conducted under PRAD conditions (Fig. 12). The results indicated these genes were significantly downregulated, highlighting their potential relevance in prostate cancer.

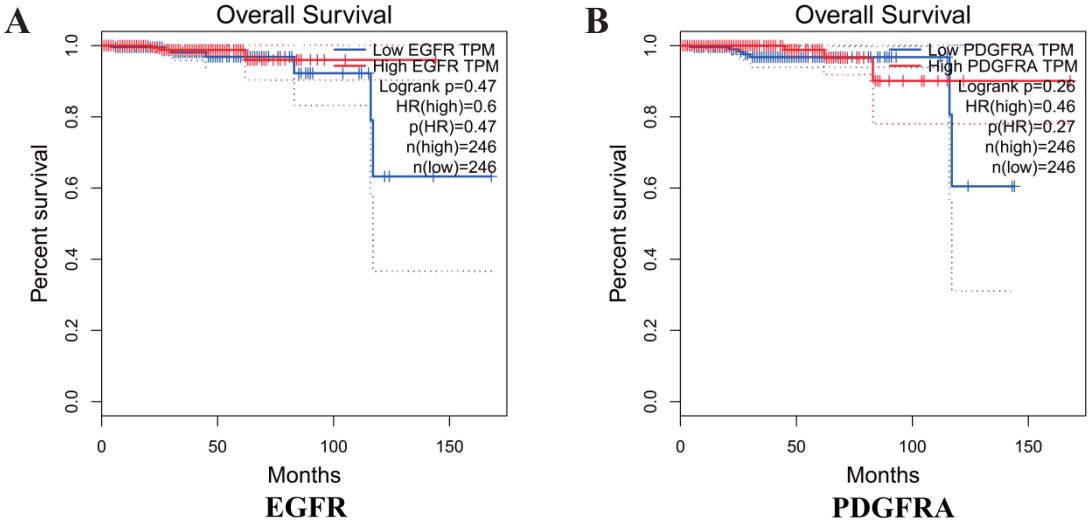

Fig. 11 Survival curve of six core targets of *Corydalis yanhusuo* against prostate cancer. (A-F) EGFR, PDGFRA, PIK3CA, PIK3CD, PIK3CG, and PIK3R1. '*n*' denotes the number of cases, and '*p*' represents the *p*-value of the test

(to be continued)

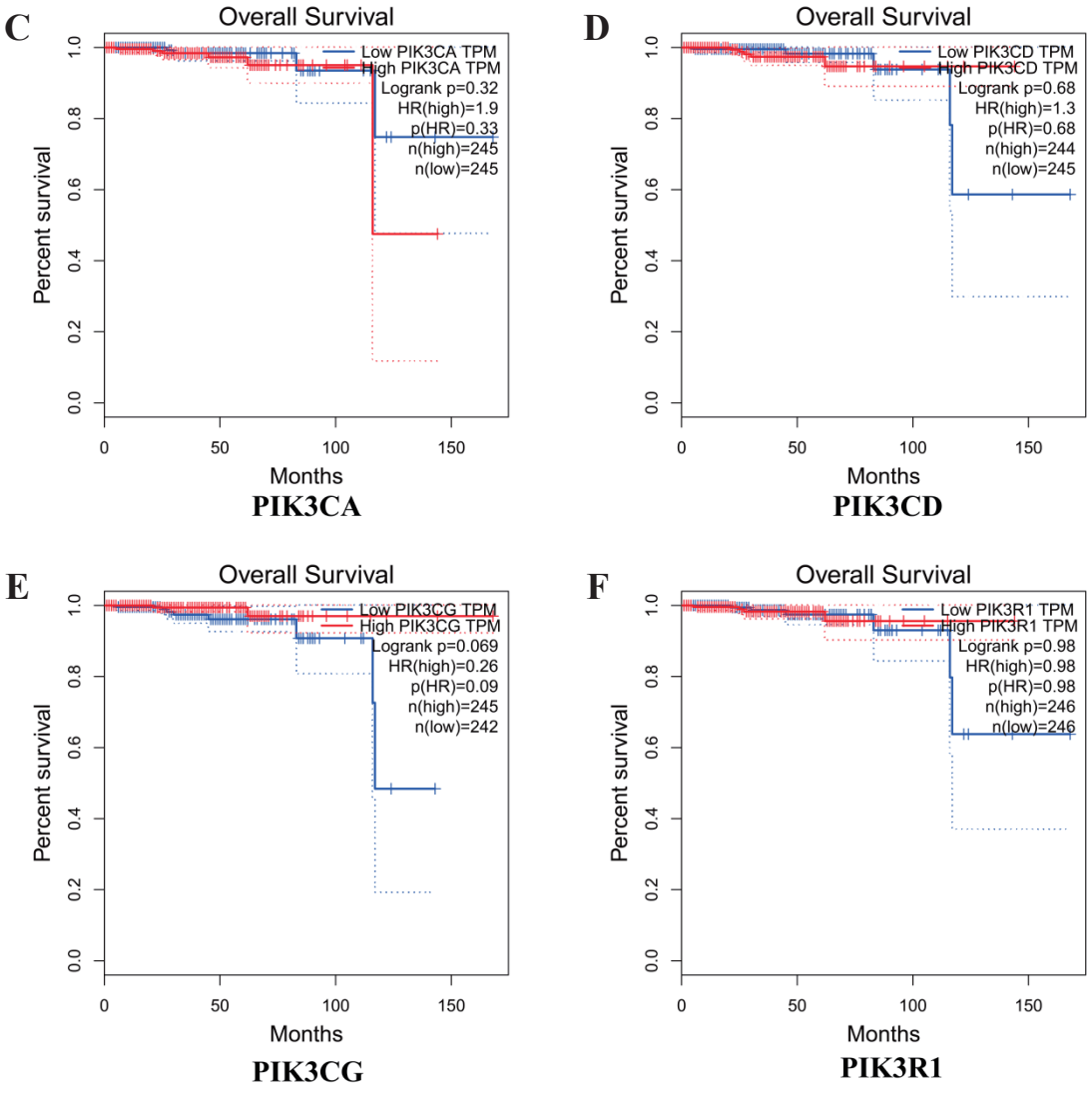

Continued Fig. 11

4 Discussion

Currently recognized risk factors for prostate cancer include age, family history, genetic mutations, prostatitis, benign prostatic hyperplasia, obesity, smoking and dietary factors [38]. The incidence and mortality rates of prostate cancer vary significantly due to race, ethnicity and geographical location. The highest incidence rates is observed in North America, Western Europe and Northern Europe, while the motality rate of African-American men is the highest [39].

With the increase of the number and incidence rate of prostate cancer cases, the curative effect of the western medicine alone is limited. It is urgent to explore the treatment of prostate cancer with integrated traditional Chinese and western medicine. Traditional Chinese medicine believes that the key pathological factors in prostate cancer are “deficiency, dampness, heat, blood stasis and

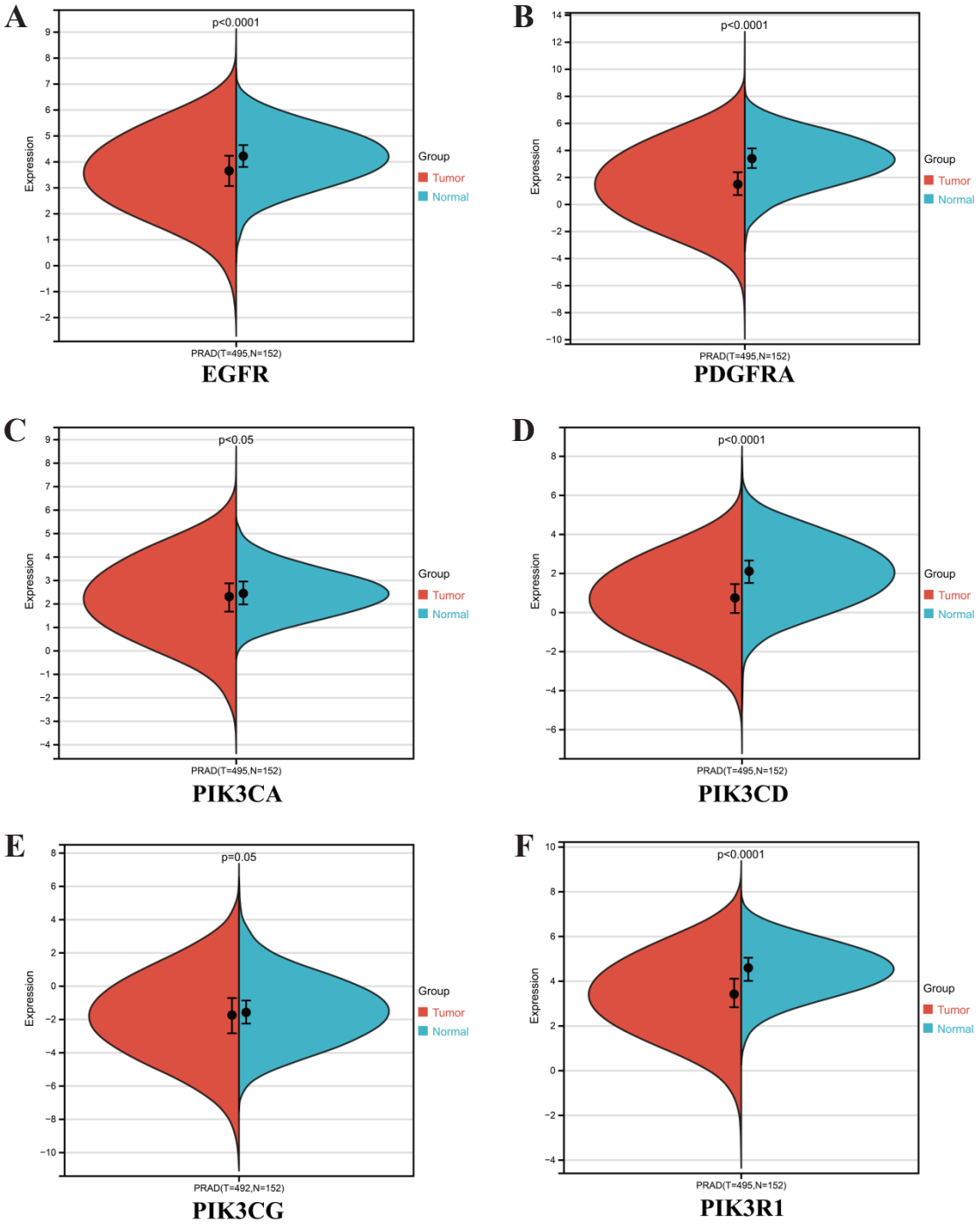

Fig. 12 Pan-cancer analysis of six core targets of *Corydalis yanhusuo* in anti-prostate cancer. (A-F) EGFR, PDGFRA, PIK3CA, PIK3CD, PIK3CG, and PIK3R1

toxicity". It adopts the principle of "warming to supplement deficiency", and *Corydalis yanhusuo* is described as "warm in nature, bitter and pungent in taste, and related to liver, spleen, and lung meridians" [40,41]. *Corydalis yanhusuo* is frequently used in many traditional Chinese medicine formulations for treating prostate cancer [42,43].

Traditional Chinese medicine has unique advantages in tumor treatment, enhancing physical resilience, improving tolerance to treatments, enhancing quality of life, reducing toxic side effects, and potentially improving treatment efficacy.

This study employed network pharmacology methods to screen 19 active chemical components, such as protopine, berberine, coptisine and stylopine, sourced from the TCMSP, TCM-ID and BATMAN-TCM databases. Protopine, identified as a novel microtubule stabilizer, induces mitotic arrest and apoptosis in hormone-resistant prostate cancer (HRPC) cells [44]. Li et al. reported that berberine inhibits androgen receptor signaling in prostate cancer, suggesting its potential as a therapeutic agent [45].

Cyclooxygenase-2 (COX-2) is frequently overexpressed in various epithelial malignancies, including prostate cancer, catalyzing the conversion of arachidonic acid into prostaglandins like prostaglandin E2 (PGE2) [46]. This further upregulates COX-2 expression via a prostaglandin transporter-dependent mechanism, promoting proliferation, migration, and invasion in prostate cancer PC3 cells [47]. Zhou et al. demonstrated that coptisine significantly inhibited nitric oxide (NO) and PGE2 production [48]. Additionally, Jang et al. showed that stylopine inhibited NO and PGE2 production in macrophages by suppressing inducible nitric oxide synthase (iNOS) and COX-2 expression [49]. Hence, coptisine and stylopine may hinder prostate cancer development through their impact on COX-2 and PGE2 expression.

GO enrichment and KEGG pathway analysis shows that signaling pathways such as the Rap1 signaling pathway, phospholipase D signaling pathway and Ras signaling pathway play crucial roles in prostate cancer. The Rap1 signaling pathway regulates integrins and cadherins, influencing cell-ECM and cell-cell adhesion dynamics [50]. In prostate cancer, Signal-Induced Proliferation-Associated 1 (SIPA1) can enhance tumor cell invasion and metastasis by inhibiting Rap1-mediated cell-ECM adhesion [51].

Studies by Noble et al. indicate that suppressing Phospholipase D2 (PLD2) expression diminishes the viability, colony-forming ability and directional motility of prostate cancer cells [52]. Research by Hong et al. highlights phospholipase D's significant role in regulating cell proliferation and tumorigenesis pathways, suggesting the phospholipase D/phosphatidic acid signaling pathway as a potential cancer treatment target [53].

Research findings from Strittmatter et al. suggest that differences in Ras/ERK or PI3K/AKT signaling may influence abnormal ETS Transcription Factor ERG (ERG) expression in prostate cancer, impacting its physiological functions [54]. Additionally, Weber et al. found that Ras signaling pathway activation reduced prostate cancer cell dependency on androgens, potentially accelerating disease progression [55].

Through gene differential analysis, key targets such as EGFR, PDGFRA and PIK3CA were identified, highlighting the multi-target characteristics of traditional Chinese medicine treatments. Zhou et al. discovered that F-box and WD-repeat domain-containing 2 (FBXW2) suppressed prostate cancer proliferation and metastasis by promoting EGFR ubiquitination and degradation [56]. Rossini et al. demonstrated through cell and mouse experiments that EGFR overexpression in prostate cancer cells promoted

metastasis [57]. PDGFRalpha plays a crucial role in promoting the survival of prostate cancer bone metastasis and early metastatic progression. High expression of PDGFRalpha facilitates bone metastasis in prostate cancer [58]. Zhang et al. [59] found that miR-202 inhibited prostate cancer growth and metastasis by targeting PIK3CA. These findings underscore the significant roles of EGFR, PDGFRA and PIK3CA in prostate cancer onset and metastasis.

GSEA enrichment analysis revealed that the JAK-STAT, MAPK and Wnt signaling pathways were significant in prostate cancer. Interferon Induced Protein With Tetratricopeptide Repeats 5 (IFIT5) acts as a downstream effector of the JAK-STAT pathway, with its activation promoting prostate cancer stem cell characteristics through the accelerated conversion of specific microRNAs. Consequently, inhibiting JAK-STAT pathway signaling represents a novel therapeutic approach for prostate cancer [60].

Steiner et al. demonstrated through experiments that autocrine activation mediated by MAPK signaling enhanced the intrinsic tolerance of Lymphocyte antigen 6 superfamily member D (LY6D) prostate cancer cells to androgen deprivation [61]. Early intervention with MAPK inhibitors could thus mitigate the progression of castration-resistant prostate cancer.

Additionally, Murillo-Garzón et al. identified the pivotal role of Wnt signaling in prostate cancer development, showing that its activation promoted the progression from prostatic intraepithelial neoplasia (PIN) lesions to adenocarcinoma [62].

The molecular docking and dynamics simulation results indicated that coptisine, dehydrocorydalmine, bicuculline and stylopine from *Corydalis yanhusuo* exhibited strong binding to proteins such as PDGFRA, PIK3CA and PIK3CG, demonstrating low binding energies. *Corydalis yanhusuo* achieves its anti-prostate cancer effects through multiple components, targets and pathways.

5 Conclusion

This study proves via network pharmacology methods that coptisine, dehydrocorydalmine, bicuculline, and stylopine identified in *Corydalis yanhusuo* exert therapeutic effects on prostate cancer by modulating multiple signaling pathways. These pathways include Rap1, phospholipase D, Ras, JAK-STAT, MAPK and Wnt signaling pathways, and involve targets such as EGFR, PDGFRA and PIK3CA.

Author contribution

J. X conceived the study. Y. Z and J. L, investigated and analyzed the data. J. X supervised the study. J. X wrote and revised the manuscript. All authors read and agreed to publish the paper.

Funding

This study was supported by local special projects in major health of Hubei Provincial Science and Technology Department (2022BCE054), key scientific research projects of Hubei Polytechnic University (23xjz08A), and Hubei Polytechnic University · Huangshi Daye Lake high-tech Zone University Science Park Joint Open Fund Project (23xjz04AK).

Conflict of interest

The authors declare no conflict of interest.

Data availability

The processed data and raw data are freely serviced from the first and corresponding authors.

References

[1] Wang G, Zhao D, Spring DJ, et al. Genetics and biology

of prostate cancer. Genes Dev, 2018, 32: 1105-1140.

[2] Kamat AM, Huang SF, Bermejo CE, et al. Total pelvic exenteration: effective palliation of perineal pain in patients with locally recurrent prostate cancer. J Urol, 2003, 170: 1868-1871.

[3] Gartrell BA, Saad F. Pathologic fracture in patients with metastatic prostate cancer. Curr Opin Urol, 2014, 24: 595-600.

[4] Tanno T, Rabel A, Alleyne M, et al. Hepcidin, anaemia, and prostate cancer. BJU Int, 2011, 107: 678-679.

[5] Parsons BA, Evans S, Wright MP. Prostate cancer and urinary incontinence. Maturitas, 2009, 63: 323-328.

[6] Global cancer burden growing, amidst mounting need for services. Saudi Med J, 2024, 45: 326-327.

[7] Sekhoacha M, Riet K, Motloung P, et al. Prostate Cancer Review: Genetics, Diagnosis, Treatment Options, and Alternative Approaches. Molecules, 2022, 27: 5730.

[8] Ren FM, Liu Y, Zhu XF, et al. Advances in the study of resources of Corydalis medicinal materials. World J Tradit Chin Med, 2020, 15: 717-725.

[9] Zheng H, Zou XW, Wang SY, et al. Herbal Textual Research on *Corydalis yanhusuo*. J Anhui Agric Sci, 2022, 50: 139-144+148.

[10] Jiang MD, Bao WL, Xu N, et al. Isolation and purification of alkaloids from *Corydalis yanhusuo* W. T. Wang and their anti-inflammatory effects. Guangzhou Chem Ind, 2022, 50: 70-73.

[11] Wan CX, Mu Y. Observation on the effect of acupoint application of vinegar *Corydalis yanhusuo* and Lamiophlomis rotata granules combined with acupoint application in postoperative analgesia for anorectal diseases. Med Sci J Cent South China, 2023, 51: 582-584+588.

[12] Qin XP, Meng Y, Liu SC, et al. Structure-activity relationship of anti-inflammatory and analgesic effects of *Corydalis yanhusuo* W. T. Wang in Qizhi Weitong Granules. Chin J Exp Tradit Med Formulae, 1-14 [2024-04-13]. Available at: https://doi.org/10.13422/j.cnki.syfjx.20231517

[13] Alhassen L, Nuseir K, Ha A, et al. The Extract of *Corydalis yanhusuo* Prevents Morphine Tolerance and Dependence. Pharmaceuticals (Basel), 2021, 14: 1034.

[14] Gu Y, Shi W, Wang DC. Compound Yanhusuo Decoction for the Treatment of Acute Myocardial Infarction Complicated with Malignant Ventricular Arrhythmia. Henan Tradit Chin Med, 2024, 44: 259-264.

[15] Alhassen L, Nuseir K, Ha A, et al. The Extract of *Corydalis yanhusuo* Prevents Morphine Tolerance and Dependence. Pharmaceuticals (Basel), 2021, 14: 1034.

[16] Guan XF, Wang R, Qu XF, et al. Advances in the study of chemical components and pharmacological effects of *Corydalis yanhusuo* W. T. Wang. Chem Eng, 2020, 34: 57-60.

[17] Chang S, Liu ZH, Han N, et al. Study on the Alkaloids and Their Anti-tumor Activities in the Tubers of *Corydalis yanhusuo* W. T. Wang. Chin Tradit Pat Med, 2022, 44: 3507-3513.

[18] Liu TT, Zhang Z, Wang C, et al. The mechanism of action of dehydrocorydaline in the treatment of bladder cancer. J Wannan Med Coll, 2022, 41: 409-412.

[19] Hang JS, Xu KY, Zhu SY, et al. Clinical application and dosage of *Corydalis yanhusuo* W. T. Wang. Jilin J Chin Med, 2020, 40: 809-811.

[20] Ru J, Li P, Wang J, et al. TCMSP: a database of systems pharmacology for drug discovery from herbal medicines. J Cheminform, 2014, 6: 13.

[21] Chen X, Zhou H, Liu YB, et al. Database of traditional Chinese medicine and its application to studies of mechanism and to prescription validation. Br J Pharmacol, 2006, 149: 1092-1103.

[22] Liu Z, Guo F, Wang Y, et al. BATMAN-TCM: a Bioinformatics Analysis Tool for Molecular mechANism of Traditional Chinese Medicine. Sci Rep, 2016, 6: 21146.

[23] Lipinski CA. Lead- and drug-like compounds: the rule-of-five revolution. Drug Discov Today Technol, 2004, 1: 337-341.

[24] Kim S, Chen J, Cheng T, et al. PubChem in 2021: new data content and improved web interfaces. Nucleic Acids Res, 2021, 49: 1388-1395.

[25] Daina A, Michielin O, Zoete V. SwissADME: a free web

tool to evaluate pharmacokinetics, drug-likeness and medicinal chemistry friendliness of small molecules. Sci Rep, 2017, 7: 42717.

[26] Daina A, Michielin O, Zoete V. SwissTargetPrediction: updated data and new features for efficient prediction of protein targets of small molecules. Nucleic Acids Res, 2019, 47: 357-364.

[27] Stelzer G, Rosen N, Plaschkes I, et al. The GeneCards Suite: From Gene Data Mining to Disease Genome Sequence Analyses. Curr Protoc Bioinformatics, 2016, 54: 1.30.1-1.30.33.

[28] Amberger JS, Bocchini CA, Schiettecatte F, et al. OMIM.org: Online Mendelian Inheritance in Man (OMIM®), an online catalog of human genes and genetic disorders. Nucleic Acids Res, 2015, 43: 789-798.

[29] Chen X, Ji ZL, Chen YZ. TTD: Therapeutic Target Database. Nucleic Acids Res, 2002, 30: 412-415.

[30] Von Mering C, Huynen M, Jaeggi D, et al. STRING: a database of predicted functional associations between proteins. Nucleic Acids Res, 2003, 31: 258-261.

[31] Chin CH, Chen SH, Wu HH, et al. cytoHubba: identifying hub objects and sub-networks from complex interactome. BMC Syst Biol, 2014, 8 Suppl 4: 11.

[32] Huang DW, Sherman BT, Tan Q, et al. DAVID Bioinformatics Resources: expanded annotation database and novel algorithms to better extract biology from large gene lists. Nucleic Acids Res, 2007, 35: 169-175.

[33] UniProt Consortium. UniProt: the universal protein knowledgebase in 2021. Nucleic Acids Res, 2021, 49: 480-489.

[34] Berman HM, Westbrook J, Feng Z, et al. The Protein Data Bank. Nucleic Acids Res, 2000, 28: 235-242.

[35] Eastman P, Swails J, Chodera JD, et al. OpenMM 7: Rapid development of high performance algorithms for molecular dynamics. PLoS Comput Biol. 2017, 13: 1005659.

[36] Tian L, Sobtop, Version [1.0(dev3.1)], http://sobereva.com/soft/Sobtop (accessed on 10, August 2024)

[37] Maier JA, Martinez C, Kasavajhala K, et al. ff14SB: Improving the Accuracy of Protein Side Chain and Backbone Parameters from ff99SB. J Chem Theory Comput, 2015, 11: 3696-3713.

[38] Zhou Q, Tian XF, Chang DG, et al. Chinese expert consensus on integrated traditional Chinese and Western medicine diagnosis and treatment of prostate cancer and health management. Natl J Androl, 2022, 2: 941-953.

[39] Rebbeck TR. Prostate Cancer Genetics: Variation by Race, Ethnicity, and Geography. Semin Radiat Oncol, 2017, 27: 3-10.

[40] Li C, Yao Y, Li L, et al. Based on the theory of cancer toxin pathogenesis for the treatment of prostate cancer. J Beijing Univ Tradit Chin Med, 1-7 [2024-04-13].39.Available at: https://doi.org/10.3969/j.issn.1006-2157.2024.03.003.

[41] Chen KD, Cui HR, Cheng XH, et al. Pharmacological Study on *Corydalis yanhusuo* W. T. Wang. Northwest Pharm J, 2023, 38: 1-9.

[42] Liu DG, Chen QH. Chen Qihua's experience in the treatment of hormone refractory prostate cancer by stages. Mod J Integr Tradit Chin West Med, 2021, 30: 2364-2368.

[43] Yang XY, Chen QH, Cai WL, et al. Clinical Research Progress of Traditional Chinese Medicine in the Treatment of Prostate Cancer. Inf Tradit Chin Med, 2023, 40: 71-76+81.

[44] Chen CH, Liao CH, Chang YL, et al. Protopine, a novel microtubule-stabilizing agent, causes mitotic arrest and apoptotic cell death in human hormone-refractory prostate cancer cell lines. Cancer Lett, 2012, 315: 1-11.

[45] Li J, Cao B, Liu X, et al. Berberine suppresses androgen receptor signaling in prostate cancer. Mol Cancer Ther, 2011, 10: 1346-1356.

[46] Ching MM, Reader J, Fulton AM. Eicosanoids in Cancer: Prostaglandin E(2) Receptor 4 in Cancer Therapeutics and Immunotherapy. Front Pharmacol, 2020, 11: 819.

[47] Madrigal-Martínez A, Constâncio V, Lucio-Cazaña FJ, et al. PROSTAGLANDIN E(2) stimulates cancer-related phenotypes in prostate cancer PC3 cells through cyclooxygenase-2. J Cell Physiol, 2019, 234: 7548-7559.

[48] Zhou K, Hu L, Liao W, et al. Coptisine Prevented IL-

β-Induced Expression of Inflammatory Mediators in Chondrocytes. Inflammation, 2016, 39: 1558-1565.

[49] Jang SI, Kim BH, Lee WY, et al. Stylopine from Chelidonium majus inhibits LPS-induced inflammatory mediators in RAW 264.7 cells. Arch Pharm Res, 2004, 27: 923-929.

[50] Pannekoek WJ, Kooistra MR, Zwartkruis FJ, et al. Cell-cell junction formation: the role of Rap1 and Rap1 guanine nucleotide exchange factors. Biochim Biophys Acta, 2009, 1788: 790-796.

[51] Shimizu Y, Hamazaki Y, Hattori M, et al. SPA-1 controls the invasion and metastasis of human prostate cancer. Cancer Sci, 2011, 102: 828-836.

[52] Noble AR, Hogg K, Suman R, et al. Phospholipase D2 in prostate cancer: protein expression changes with Gleason score. Br J Cancer, 2019, 121: 1016-1026.

[53] Hong X, Huang J. Research progress on the role of phosphatase D in tumor development. Chin J Pharmacol Toxicol, 2023, 37: 289-294.

[54] Strittmatter BG, Jerde TJ, Hollenhorst PC. Ras/ERK and PI3K/AKT signaling differentially regulate oncogenic ERG mediated transcription in prostate cells. PLoS Genet, 2021, 17: 1009708.

[55] Weber MJ, Gioeli D. Ras signaling in prostate cancer progression. J Cell Biochem, 2004, 91: 13-25.

[56] Zhou T, Chen T, Lai B, et al. FBXW2 inhibits prostate cancer proliferation and metastasis via promoting EGFR ubiquitylation and degradation. Cell Mol Life Sci, 2022, 79: 268.

[57] Rossini A, Giussani M, Ripamonti F, et al. Combined targeting of EGFR and HER2 against prostate cancer stem cells. Cancer Biol Ther, 2020, 21: 463-475.

[58] Russell MR, Jamieson WL, Dolloff NG, et al. The alpha-receptor for platelet-derived growth factor as a target for antibody-mediated inhibition of skeletal metastases from prostate cancer cells. Oncogene, 2009, 28: 412-421.

[59] Zhang S, Cai J, Xie W, et al. miR-202 suppresses prostate cancer growth and metastasis by targeting PIK3CA. Exp Ther Med, 2018, 16: 1499-1504.

[60] Lo UG, Chen YA, Cen J, et al. The driver role of JAK-STAT signalling in cancer stemness capabilities leading to new therapeutic strategies for therapy- and castration-resistant prostate cancer. Clin Transl Med, 2022, 12: 978.

[61] Steiner I, Flores-Tellez T, Mevel R, et al. Autocrine activation of MAPK signaling mediates intrinsic tolerance to androgen deprivation in LY6D prostate cancer cells. Cell Rep, 2023, 42: 112377.

[62] Murillo-Garzón V, Kypta R. WNT signalling in prostate cancer. Nat Rev Urol, 2017, 14: 683-696.